Wiley
Structural Control and Health Monitoring
Volume 2025, Article ID 5605927, 17 pages
https://doi.org/10.1155/stc/5605927

WILEY

Research Article

Physics-Informed Digital Twins: Enhancing Concrete Structural Assessment Based on Point Cloud Data

Honghong Song,[1] **Xiaofeng Zhu**,[2] **Haijiang Li**,[2] **Gang Yang**,[3] **and Tian Zhang**[3]

[1]*School of Mechanics and Aerospace Engineering, Dalian University of Technology, Dalian, China*
[2]*School of Engineering, Cardiff University, Cardiff, UK*
[3]*College of Transportation Engineering, Dalian Maritime University, Dalian, China*

Correspondence should be addressed to Haijiang Li; lih@cardiff.ac.uk and Gang Yang; yanggang@dlmu.edu.cn

Received 3 January 2024; Revised 3 January 2024; Accepted 12 June 2025

Academic Editor: Mohamed Ichchou

Finite element modeling is widely regarded as an effective method for simulating structural responses, but maintaining geometrical consistency with damaged physical structures remains insufficiently explored. This paper proposes a new physics-informed digital twin framework for concrete structure modeling and implements the twinning/synchronization process between the physical model and its counterpart finite element analysis (FEA) model. This framework starts with point cloud scanning for damage and point cloud processing. Subsequently, a direct mapping method called Voxel–Node–Element (VNE) is proposed, which can improve mapping efficiency and reduce mapping errors. Furthermore, a multiscale modeling method is adopted to enhance digital twin modeling updates, dramatically reducing the number of elements and improving computational efficiency. An experimental case study was conducted to evaluate this method, showing good alignment between point cloud and physics models with a geometric error of less than 5%. Additionally, computational efficiency was improved by 95% compared to traditional methods. This method can also be used for full-scale structure modeling, which was validated in the case of damage updates for large bridges. This study enables a highly accurate and efficient method for updating digital twin models. This capability was validated through damage updates applied to large-scale bridge structures.

Keywords: concrete damage; finite element model; physics-informed digital twin; point cloud

1. Introduction

The occurrence of natural disasters such as earthquakes often causes serious damage such as cracks or spalling to reinforced concrete or concrete structures, as shown in Figure 1, which may endanger human safety. Subsequent search and rescue operations afterward can still be perilous because of uncertain knowledge of structural stability. Currently, the diagnosis of concrete structures relies on manual inspection, measurement, and empirical assessment, which are inefficient and error-prone [1, 2]. Handling the large volume of bridge inspections and evaluations is time-consuming. Delayed or inaccurate structural assessments can result in significant property damage and loss of life.

Digital twin (DT) technology provides a promising solution [5–7]. Its objective is to generate a precise virtual rendition of the physical world in the digital realm and to enhance this representation with new functionalities such as assessment and prediction [8–11]. Within structural analysis, DTs play a pivotal role by encapsulating explicit knowledge of structural behavior, damage patterns, and other relevant factors [12–15]. This includes amalgamating structural models with damage data to establish a cohesive representation [16–19]. In particular, applying DT approaches that incorporate simulated or machine learning-based models provides a practical means of addressing this challenge.

Machine learning-driven DTs provide significant advantages in predicting the overall performance of a structure

Figure 1: Significant damage at the concrete girder (Images from Google search [3, 4]).

while reducing time and computational cost. For example, Mousavi et al. [20] proposed a novel DT-based method for learning damage-sensitive features from data generated from various scenarios of a simulated simple Floating Wind Turbine (FWT) model, enabling rapid damage detection in a complex FWT model. Machine learning models that incorporate physical information demonstrate greater advantages, particularly with limited input data. For instance, Radbakhsh et al. [21] developed DTs driven by physics-informed neural networks (PINNs), which combine physical information with data-driven machine learning models and have effectively captured structural deflections.

Physics-informed digital twins (PIDTs), such as those based on finite element (FE) structural models, play a critical role in capturing the local mechanical properties of a structure, particularly the stress changes in the cross section due to local damage [22–24]. In the field of PIDT updating, computer vision-based methods have shown significant advantages. Firstly, data derived from cameras and scanners can enable remote inspections via unmanned aerial vehicles (UAVs) [1, 25], thereby improving the efficiency and safety of inspections. Secondly, images and point cloud data provide rich visual information for structural assessment. Furthermore, computer vision technology offers the possibility of automated damage identification, localization, and measurement of potential damage through the processing of images and point cloud data [26–28]. For example, Jiang et al. [25] developed a vision-guided unmanned aerial system with a lightweight convolutional neural network to detect and locate bridge cracks, spalling, and corrosion.

However, there are still research gaps in DT updating based on image and point cloud data. On the one hand, image-based FE model updating can offer a richer and more intuitive visual representation for structural assessment [29, 30]. For example, Zhang et al. [29] proposed a method for integrating cracks from 2D images into a 3D model to automatically generate a FE model. Cracks are extracted in 2D images, and 3D models are obtained by point cloud processing. A registration algorithm called Iterative Closest Point-based Direct Linear Transformation is proposed to project cracks onto 3D models, for the automatic generation of FE models. However, 2D images lack depth information about the cracks. On the other hand, point clouds provide a three-dimensional framework, geometry, and location information of the damage, which can compensate for the limitations of image data [31–35]. Researchers [36, 37] have obtained complete point cloud data of structures through full-scale scans and subsequently applied reverse 3D modeling techniques to develop new FE models. Although this method has yielded promising results, it also presents several limitations. First, the automation level for shape customization and accurate geometric fitting remains low. Second, full-scale scanning struggles to capture the fine details of damage. Kong et al. [38] proposed a more practical method by calculating the convex hull volume of point clouds and combining it with image-based damage localization to update the damage information locally. This method avoids the complexity of processing global point cloud data and improves the accuracy of damage quantification. However, convex hull volume calculation is less adaptable to complex geometries. For example, convex hull algorithms can only generate the minimal convex envelope surrounding the damaged area, making it difficult to capture complex geometries on the damage surface—particularly concave regions and fine cracks. Moreover, error accumulation significantly affects the accuracy of damage quantification.

Based on the aforementioned research gaps, this paper proposes a new research question: How can a direct link be established between point cloud models and FE models, enabling efficient updating of damage information within the FE model? To address this issue, the study introduces a PIDT updating method. The approach enables efficient and high-precision interaction between local point cloud data and the FE model through a novel mapping technique combined with multiscale modeling. The primary contributions of this study are as follows: (1) A comprehensive framework for PIDT damage updating is proposed, which demonstrates the process of data collection, damage mapping, model synchronization, and the updating process after damage repair. (2) A new damage mapping method, Voxel–Node–Element (VNE), was developed, which achieves direct and automatic mapping between point cloud data and FE models; additionally, this method not only accounts for the volume of damage but also provides detailed information on the shape and direction of the damage. (3) Multiscale modeling is introduced to enhance DT model synchronization and computational efficiency. This study establishes a direct mapping between the point cloud and FE models, eliminating the need for complex damage volume calculations. It enables full-dimensional damage updates, providing higher-quality information for concrete damage assessment and improving decision-making accuracy.

The article is organized as follows: (1) The framework of PIDT (Section 2); (4). Introduces the proposed VNE method for PIDT updating (Section 3); (5) Multiscale modeling method enhanced PIDT modeling (Section 4); (6) Experimental case validation (Section 5); (7) Discussion and conclusion (Section 6).

2. Framework of PIDT

Accurate assessment of concrete structures requires the use of high-fidelity structural analysis models. These models must take into account both the initial (design-phase) mechanical properties and real-time (operational-phase) damage data. DTs are designed to replicate the actual state of

physical entities and include purely data-driven or physically based DTs (e.g., detailed FE models) [17]. A key challenge in PIDT models is maintaining high fidelity, meaning that the models should reflect the current condition of the structural entity to achieve accurate state estimation. Therefore, a federated model between physics-based virtual models and its reality version is proposed.

In this study, a PIDT is proposed based on FE parametric modeling and scan-based point cloud data, which satisfies the framework of the DT [19], as shown in Figure 2. The FE model is considered a physics-informed virtual model because its construction incorporates physical knowledge such as material properties, geometry, boundary conditions, and governing equations to simulate real-world structural behavior. In this framework, real-time damage information is captured through point cloud scanning, which provides a comprehensive representation of the structure's spatial and geometric features. These data are then aligned and mapped onto the FE model to generate a virtual representation that closely mirrors the physical structure—namely, the PIDT. This model enables more accurate and intuitive structural evaluation, thereby supporting informed decision-making and efficient maintenance planning.

The PIDT model updating methodology is shown in Figure 3. The presented approach requires an initial model in the form of an as-built or designed 3D FE model of the structural components. The main steps are as follows.

The first step is data acquisition and processing. The initial step involves comprehensive data acquisition, where damage information is extracted from point cloud data collected via scanning technologies. These data primarily encompass the precise location and geometric characteristics of the damage present in the structure. To accurately determine the damage location, a radar positioning system is employed. This system not only pinpoints where the damage occurs but also informs the construction of a micromodel within the DT framework. The micromodel serves as a detailed representation of the damaged area, ensuring that subsequent analyses reflect the true state of the structure. In parallel, the geometric information derived from the point cloud data is encapsulated within a damage skeleton model. This model is generated after rigorous point cloud processing, which involves filtering and refining the data to isolate damage features. The resulting skeleton model provides a simplified yet accurate representation of the damage's geometry, enabling further analysis and mapping.

Next comes damage mapping by the proposed VNE method and PIDT synchronization based on a multiscale hybrid finite element analysis (FEA) model. The VNE method plays a critical role by achieving direct and automatic mapping between the processed point cloud data and the FE models. It not only quantifies the volume of the damage but also captures its intricate geometric and directional characteristics. This comprehensive mapping ensures that the DT model reflects the true nature of the damage, enhancing both accuracy and reliability. PIDT synchronization further refines this process by integrating the updated damage information into the existing structural models, enabling for a cohesive representation that is responsive to the physical conditions of the structure. The specific implementation details of both the VNE method and the PIDT synchronization process will be elaborated in Sections 3 and 4.

Following the completion of these repairs, the DT model is updated once again to incorporate the revised damage locations and geometries. This iterative updating process is crucial, as it ensures that the DT remains an accurate reflection of the physical structure, thereby supporting ongoing monitoring and assessment efforts.

3. The Proposed Damage Mapping Method

The VNE method is proposed for damage updating in DT models. It directly maps voxels in the point cloud model to nodes in the FE model, enabling efficient and accurate damage updates.

The VNE method involves two key steps, starting with damage localization. As illustrated in Figure 4, one end of the structure is designated as the take-off point for the UAV, and its coordinates are recorded. The node in the FE model corresponding to the UAV take-off point is located, and its coordinates are determined. Based on the relationship between these two coordinate systems, the point cloud coordinates are batch-processed to align with the FE model coordinate system.

The next step involves damage mapping, as illustrated in Figure 5. The point cloud model comprises numerous voxels, each defined by 3D coordinates. Similarly, the FE model consists of nodes and elements, with each node also associated with 3D spatial coordinates. Based on this, this paper proposes to map voxel coordinates to element node coordinates, establishing a direct link between the point cloud model and the FE analysis model. The point cloud model consists of multiple voxels, each with three-dimensional coordinates. The FE model is composed of multiple nodes and corresponding elements, with each node also having three-dimensional coordinates. Based on this, this paper proposes mapping the voxels with nodes by coordinates, establishing a direct link between the point cloud model and the FE analysis model. As point clouds only offer information on the component's surface, and both the damaged and internal healthy areas are blank in the point cloud, identifying damaged elements by simply matching the point cloud to the FE model is very laborious and time-consuming. An automated FE model updating method is proposed and implemented based on Python to update the FE model efficiently. During this process, the inputs include the voxel coordinates from the damage skeleton, the corresponding FE node coordinates, and the element numbers within the relevant spatial range. The output is a list of all FE elements that correspond to the damaged region, as shown in Table 1. In addition, an ANSYS parametric design language (APDL) for FE model updating is automatically generated using Python.

In addition, the Birth and Death element method, which is widely used for modeling material failures such as cracks or spalling [18, 39], provides an effective way to represent vacant damaged regions in structures. When the birth and

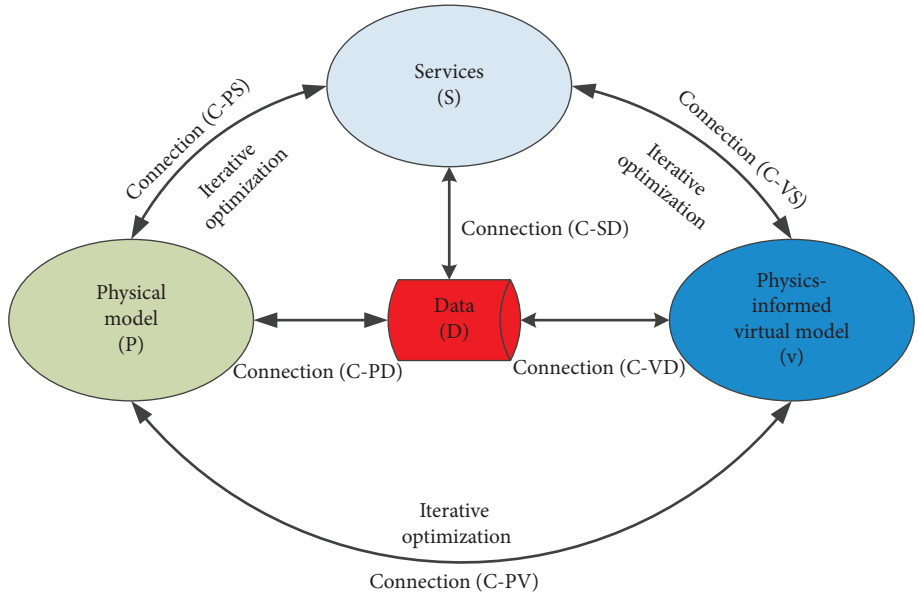

Figure 2: The components of physics-informed digital twin model.

death capability is used, the specified element is deactivated. A deactivated element remains in the model but contributes only a near-zero value to the overall matrix in terms of stiffness, conductivity, or other relevant properties. Any solution-dependent state variables (such as stress, plastic strain, creep strain) are set to zero. Deactivated elements do not contribute to the overall mass or capacitance matrix and do not generate any load vectors such as pressure, convection, or gravity forces [40]. There are two advantages to modeling the damaged region using the Birth and Death element method. Firstly, the killed elements are not deleted, but their stiffness matrix is multiplied by a small factor so that their effect on the overall behavior of the model is negligible and thus does not affect the convergence of the structural calculations. Secondly, when the damage is repaired, the killed elements can be reactivated.

4. Multiscale Modeling Enhanced DT Model Synchronization

The VNE method proposed in this paper ensures the accuracy and efficiency of updating the DT model. To further improve analysis efficiency, this paper proposes a DT modeling approach supported by a multiscale modeling method. The essence of multiscale modeling lies in the issue of deformation coordination at the connections between different types of elements. This involves simultaneously incorporating various sizes and types of elements into the same FE model. For large structures, established FE models typically operate at a single macroscopic scale. For example, in the modeling of long-span prestressed bridge structures, BEAM elements are commonly employed to simulate the overall bridge response. While such models are deemed sufficient for the initial bridge design phase, they exhibit limitations in capturing detailed distributions within specific cross sections. To emphasize local details, using a fine mesh size for the entire structure would lead to a notable increase in the number of elements and nodes, significantly affecting the computational efficiency of the structural analysis.

To achieve a balance between the accuracy of damage updates and computational efficiency, this study utilizes multiscale methods and novel element regeneration approaches to develop PIDT models. A multiscale model refers to the combination of large-scale elements representing the overall structure and small-scale elements capturing local details. Large scale refers to the characteristic dimensions within a range of 10 m, while small scale refers to dimensions within 10^{-3} m. The multiscale modeling method allows simulation of stress distribution, crack propagation, and other phenomena at the small scale, while employing large-scale analysis to capture the overall structural elastic behavior. Thus, a balance between the overall structure and local details is achieved, ensuring consistency in structural behavior. The fundamental principle of this implementation, exemplified by a static problem, is mathematically described as follows:

For general engineering structures, the matrix static equilibrium equations can be expressed as

$$K^L X^L = F^L. \tag{1}$$

In the equation, K^L represents the overall structural stiffness matrix, X^L denotes the nodal displacement vector, and F^L represents the load vector.

Selecting critical local components of the structure as the focus, and regarding them as small-scale models, these components are treated as substructures. At this point, the stiffness matrix of the local detailed region, along with the corresponding structural displacement and load matrices, are as follows [41]:

$$\begin{bmatrix} K_{BB} & K_{BS} \\ K_{SB} & K_{SS} \end{bmatrix} \begin{bmatrix} X_B \\ X_S \end{bmatrix} = \begin{bmatrix} F_B \\ F_S \end{bmatrix}. \tag{2}$$

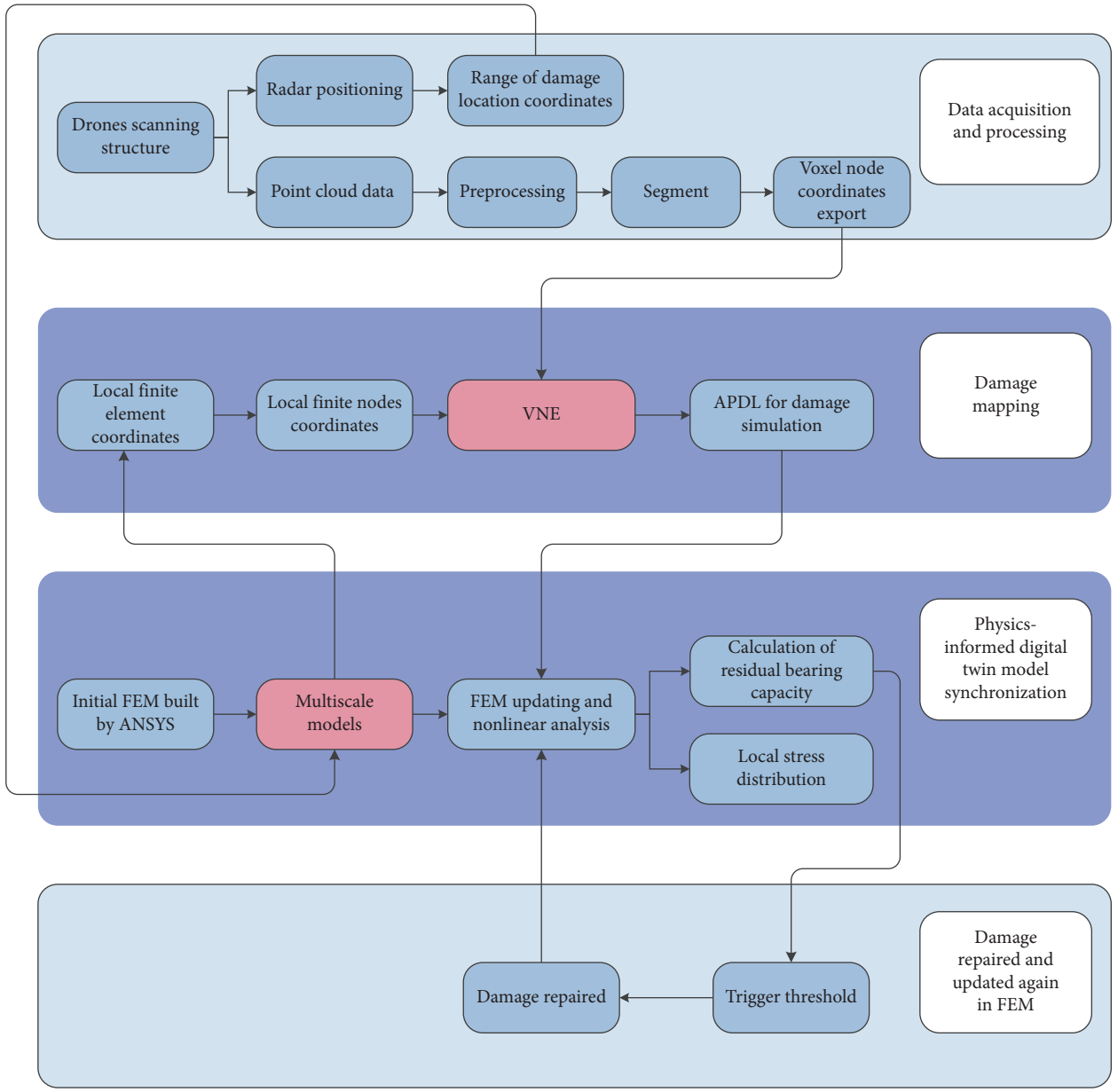

FIGURE 3: The proposed synchronization method for a physics-informed digital twin model.

In the equation, X_S represents the nodal displacement vector simulated at a small scale within the local region. X_B is the nodal displacement vector on the interface between the small-scale and large-scale models, where subscript S indicates internal nodes at the small scale, and subscript B indicates nodes on the interface associated with the small-scale structure within the large-scale structural model. The stiffness matrix K and the load vector F are also expressed in their respective block matrix forms.

Expanding equation (2) yields:

$$K_{BB}X_B + K_{BS}X_S = F_B, \tag{3}$$

$$K_{SB}X_B + K_{SS}X_S = F_S. \tag{4}$$

The internal nodal displacements of the small-scale simulated substructure can be obtained from equation (4):

$$X_S = K_{SS}^{-1}\left(F_S - K_{SB}X_B\right). \tag{5}$$

Substituting equation (5) into equation (3) yields the equation representing the aggregated internal degrees of freedom for the locally simulated small-scale structure:

$$\left(K_{BB} - K_{BS}K_{SS}^{-1}K_{SB}\right)X_B = F_B - K_{BS}K_{SS}^{-1}F_S. \tag{6}$$

Equation (6) can be expressed in an equivalent form:

$$K^*X^* = F^*, \tag{7}$$

where

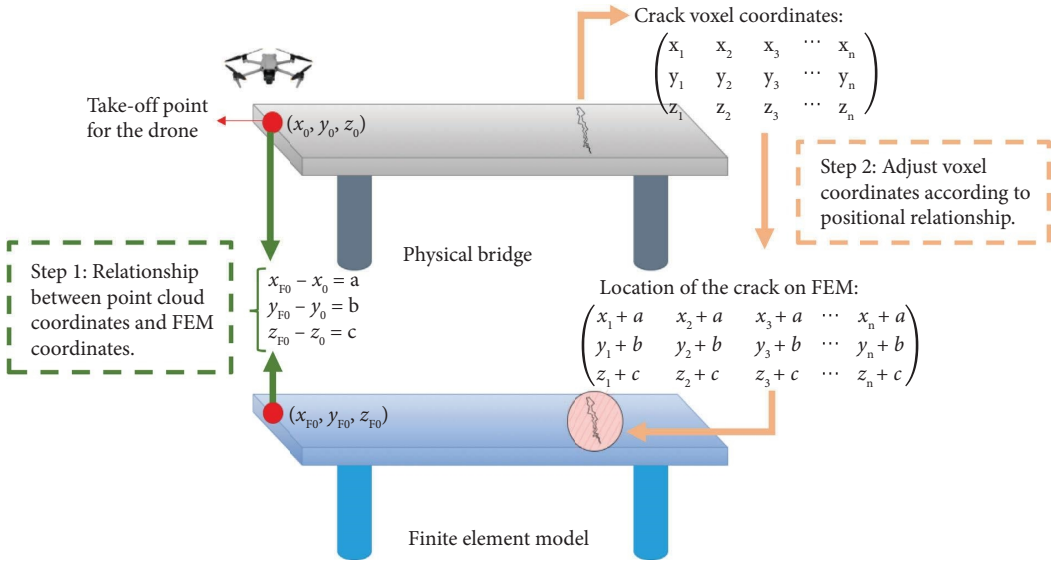

Figure 4: Schematic diagram of damage position.

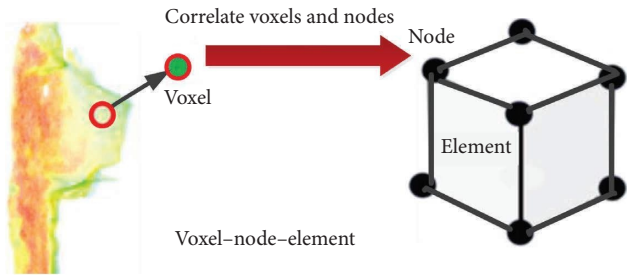

Figure 5: The proposed Voxel–Node–Element method for damage mapping.

$$K^* = \left(K_{BB} - K_{BS}K_{SS}^{-1}K_{SB}\right), \tag{8}$$

$$F^* = F_B - K_{BS}K_{SS}^{-1}F_S, \tag{9}$$

$$X^* = X_B. \tag{10}$$

In the equation, K^* and F^* are, respectively, the stiffness matrix and load vector of the local details of the small-scale model after condensation.

The specific implementation process of damage updating based on a multiscale model is shown in Figure 6. Firstly, an initial macroscopic FEA model, which is dependent on the design parameters and has a large mesh size, must be built. Then, the location of the multiscale model is identified based on the damage positions. Subsequently, the original elements at the damage location are deleted, and new elements, such as solid elements, are created to align with simulation objectives, forming a fine mesh in the damaged region. Following this, the newly generated elements are coupled with the initial model. In the final step, micromodel elements and node information are exported to facilitate damage updating, with the Birth and Death element method employed to model damage vacancies.

5. Experimental Validation

5.1. Point Cloud Data Acquisition and Processing. This case study compares the change in ultimate structural capacity after damage restoration using a plain concrete beam as an example. The beam size is $75 \times 75 \times 255$ mm. It is simply supported and subjected to third-point loading, as shown in Figure 7. The compressive strength of the cubic specimen prepared from the same batch of concrete is 43 MPa.

In this case study, damage was simulated by introducing a predefined notch into the specimen. A point cloud of the notch was then acquired using an Intel RealSense L515 scanner in the laboratory, as shown in Figure 8. The scanner has a resolution of 640×480 and a frame rate of 30 fps.

The scanning process begins with adjusting the distance between the scanner and the target object to ensure optimal scanning range and clarity. In this case, the distance between the scanner and the target was approximately 50 cm. The scanner is then aligned with the preset damage location of the concrete bending beam, and the scanning process is initiated. The scanner continuously captures the point cloud data of the target surface at a set resolution and frame rate. As the preset damage is a notch, the scanner needs to ensure complete coverage and capture the point cloud information of this area during the scanning process.

The process of capturing the damaged skeleton is implemented through the CloudCompare software [42] and consists of several key steps, as shown in Figure 9. First, the critical region of the constructed damage is segmented using crop and segment tools in CloudCompare software. Then, denoising is applied to improve the quality and accuracy of the point cloud model. Next, segmentation based on crack depth is performed to obtain a point cloud skeleton with clearer edges of the damage openings. Finally, key points are manually annotated to refine the crack skeleton and generate an accurate damaged skeleton model.

Table 1: Python-based VNE method implementation process.

Input: Node coordinate, point cloud coordinate, and element information (element number and its node number).
Output: The killed element number and APDL command stream.

```
1. //Step1. Open node coordinate file and point cloud coordinate file
2. N.x, N.y, N.z ⟵ Node Coordinate
3. P.x, P.y, P.z ⟵ Point Cloud Coordinate
4. En ⟵ Element node number
5. E ⟵ Element number
6. //Step2. Preprocess coordinate files.
7. Remove the content that is not related to the coordinates
8. //Step3. Set the coordinate tolerance for mapping
9. tor_x ⟵ 0.5
10. tor_y ⟵ 0.5
11. tor_z ⟵ 0.5
12. //Step4. Determine the scope of the search
13. set list node an empty list
14. for (each point in point cloud) do
15.    if (|P.x − N.x| <= tor_x ∧ |P.y − N.y| <= tor_y ∧ |P.z − N.z| <= tor_z) then
16.       add P into node list
17.    end if
18. end for
19. //Step5. Search element number
20. set list element an empty list
21. for (each node in node list) do
22.    for (each element in E) do
23.       if (node in En) then
24.       add E into element list
25.       end if
26.    end then
27. end then
28. //Step6. Generate the APDL command stream file
29. Create a new empty txt file
30. for (each element in element list) do
31.    add a new line with content ('ESEL,a,,,'+str(element))
32.    add a new line with content (Ekill, ALL)
33. end for
34. save txt file as the output file
```

Subsequently, a spatial down sampling method is employed, as illustrated in Figure 10, where different minimum point cloud spacing values affect the model's performance. It is observed that when the minimum spacing value is set to less than 0.002 m, the complete damage contour can be captured, and reducing the minimum spacing value enhances the clarity of damage details. To ensure that the point cloud model accurately captures the damage contour, the FE mesh density should be set to match the minimum point cloud spacing, thereby maintaining the accuracy of the damage model update. In this case, a minimum spacing of 0.001 m strikes a balance between capturing damage details and managing FE mesh complexity.

5.2. DT Model Synchronization. After the damage information in the point cloud model is extracted, the initial FE model will be updated by using the multiscale modeling and the new element regeneration methods. All the FE models in this paper are built using ANSYS software [43], whose parametric design language (APDL) offers efficient modeling and structural analysis capabilities. The initial FE model based on the BEAM element is shown in Figure 11. Following the method described in Section 4, the elements at the damage location in the initial model were first removed and then new elements were created as required.

In this case study, the solid element was used to replace the original beam element. The solid element is capable of cracking in tension and crushing in compression. For example, in concrete applications, the solid capability of the element can be used to simulate the ability of concrete to crack (in three orthogonal directions), crush, plastic deform, and creep. The most important aspect of the element is the treatment of nonlinear material properties, including large deformations and plastic deformations.

Then, an appropriate coupling method is selected to link the small-scale and large-scale models, as well as to connect the newly generated elements with the initial ones. There are several methods for connecting beam and solid elements in ANSYS [28–30] to support multiscale model building, for example:

1. Contact Interface method. This method uses contact interfaces to model the nonlinear contact behavior between different parts, which is computationally expensive and requires careful tuning and validation of the contact parameters.

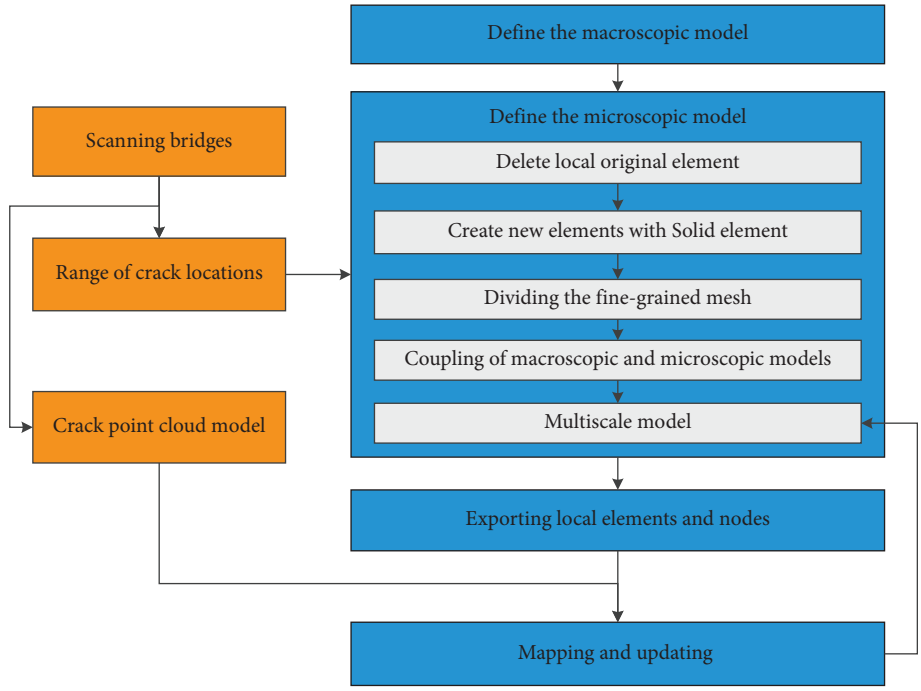

Figure 6: Multiscale modeling enhanced physics-informed digital twin modeling.

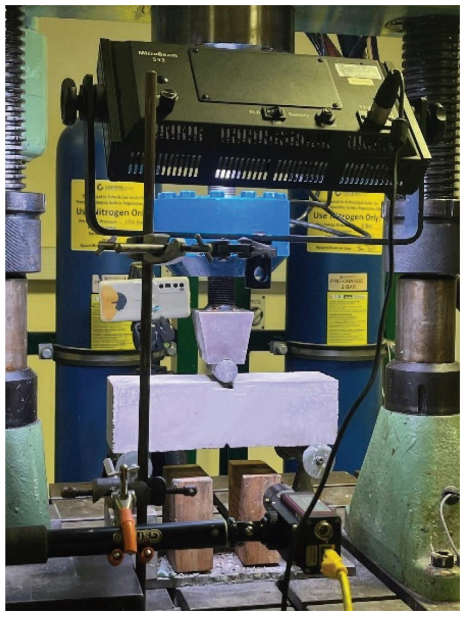

Figure 7: Experimental setup diagram.

Figure 8: Scan scene layout.

2. Multipoint Constraint method. This method is often used to connect rigid bodies or to simulate constraints.
3. Cohesive Zone Model (CZM) method. This method has been applied to model complicated microcrack initiation, propagation, branching, coalescence, and localization into macrocracks in materials similar to concrete; in addition, this method often be used to simulate the quasi-brittle fracture of concrete.
4. Rigid Link method. This method efficiently handles simple connections and constraints without considering relative motion. However, it cannot account for nonlinear behavior within the connection cross section.

In this case study, we focus solely on the effect of cracks on the surrounding stress distribution. The Rigid Link method is employed to construct the multiscale model. However, it should be noted that this method is just one example and does not represent the only approach. The specific linking method should be selected flexibly based on research requirements. For instance, if exploring crack extension behavior, the CZM proposed in [23] can be utilized. Additionally, for studying the fracture behavior of concrete, the plasticity model described in [24] can be employed.

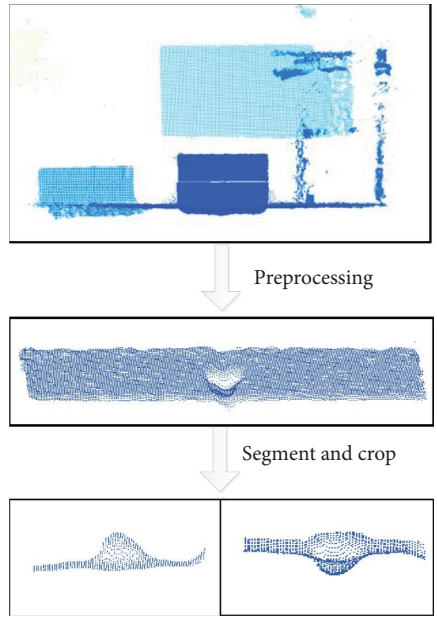

Figure 9: Point cloud processing and damage extraction.

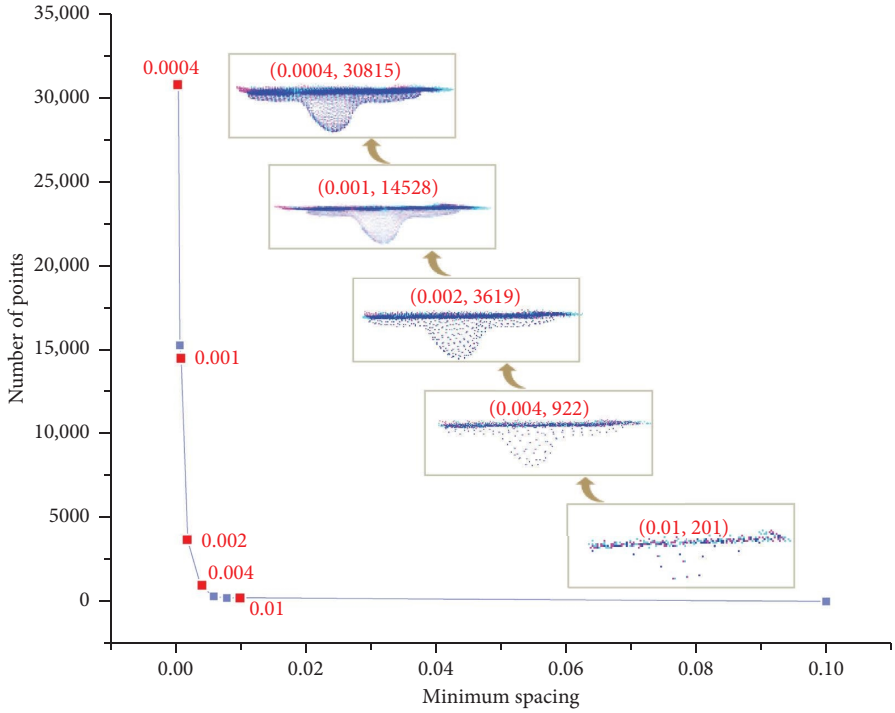

Figure 10: The influences minimum spacing of point cloud.

Upon completion of the multiscale modeling, a damage update will be performed. Figure 12 shows the PIDT model, which demonstrates that the proposed VNE damage updating method can incorporate damage into the FE model with full spatial resolution and fine granularity.

5.3. Geometric Mapping Results. To demonstrate the superiority of the proposed VNE method, this section presents and compares its geometric mapping performance. Firstly, as illustrated in Figure 13, the three-dimensional shape of the damage is compared between the point cloud model and the updated FE model. Figure 14 illustrates a comparison between the update results with and without consideration of the internal shape of the damage. Comparative results show that the VNE method has an excellent ability to accurately replicate the full-dimensional geometric features of damage compared to existing methods. The high-fidelity mapping ensures that even the intricate details of the damage geometry are preserved, thereby enhancing the

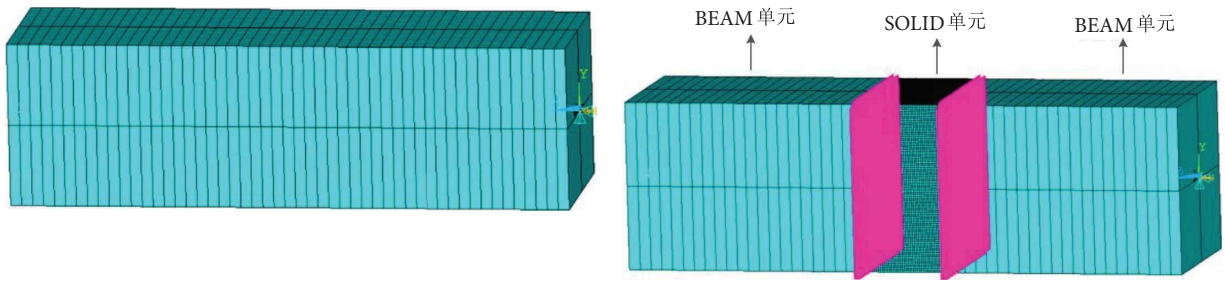

FIGURE 11: The comparison between the Initial FE model and the multiscale model. (a) Initial FE model with BEAM element. (b) The multiscale model with different element types.

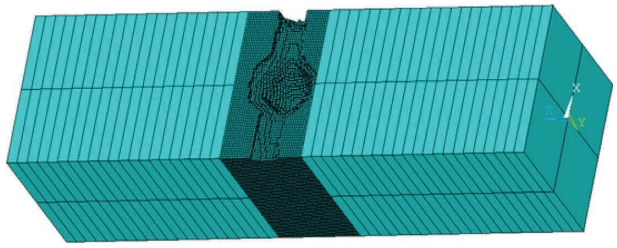

FIGURE 12: Physics-informed digital twin model.

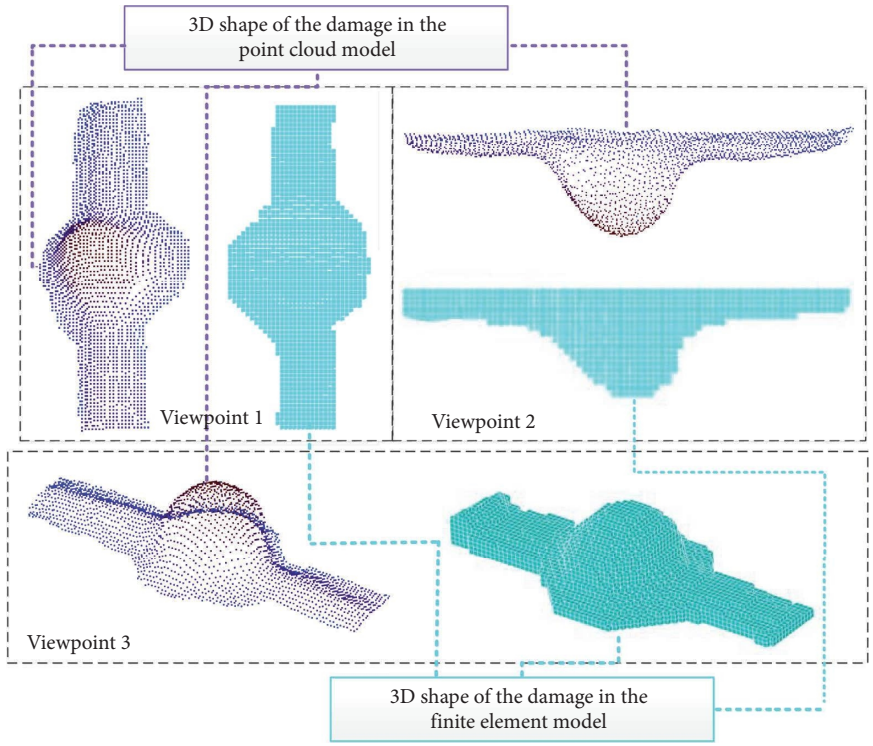

FIGURE 13: Comparison of damage shapes in point cloud and finite element models.

precision and reliability of the DT model in capturing and representing damage features. This robust replication capability underscores the effectiveness of the VNE method in maintaining the integrity of damage information during the transition from point cloud data to FEA.

Furthermore, this section compares the results of the VNE method with experimental measurement, as shown in Table 2. The volume of the crack was set experimentally to be 12,630 mm^2. The volume of the damage in the point cloud model was 11,600 mm^2. After applying the VNE updating

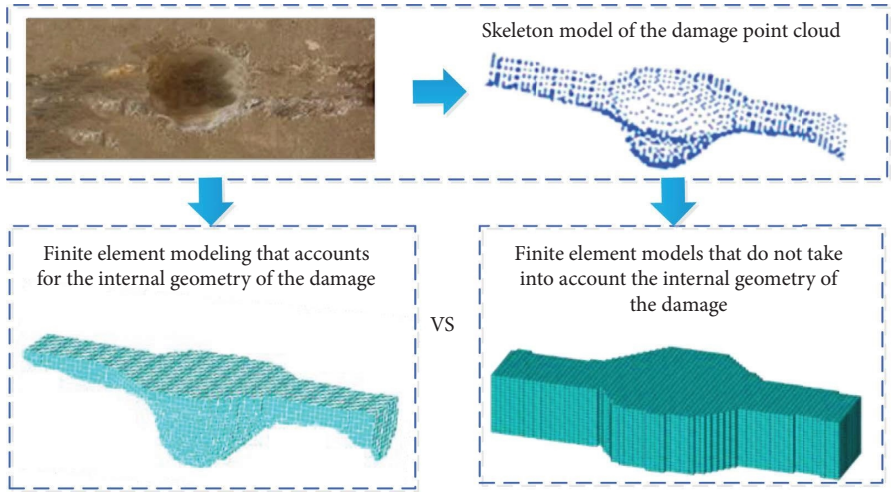

Figure 14: Comparison of finite element models with or without consideration of damaged internal geometry.

Table 2: Damage mapping results geometric comparison.

Working condition	Volume (mm^3)
Damage shape in the specimen	12,630
Damage shape in the point cloud model	11,600
The damage shape in FEM updated by the proposed VNE method	12,002

method, the volume of the damage in the FE model was 12,002 mm^2. Therefore, a comparison with the actual damage volume shows that the VNE method has a mapping error of 4.9%, while the comparison with the damage volume from the point cloud model yields a mapping error of 3.5%.

5.4. Structure Analysis Results. This section focuses on updating the structural analysis after the geometric information has been updated. In this process, the elements in the damaged area are first processed to simulate the vacancy of cracked or spalled concrete by setting up the living and dead elements in ANSYS [40]. Figure 15 illustrates the changes in the strain field when damage is incorporated into the structural analysis. The inclusion of damage significantly alters the stress distribution, with the location of the maximum stress shifting to the current position of the damage after the model update.

The ultimate loads of the FE model with damage updating, the FE model without damage updating, and the experimental specimen were compared. The ultimate load for the experimental specimen was determined through a three-point bending test. During this test, a gradually increasing load was applied at the mid-span of the specimen, and the mid-span displacement was measured using a Linear Variable Differential Transformer (LVDT). The peak load observed in the test was considered the ultimate load.

For the FE models, the ultimate load capacity was calculated by applying the same boundary conditions as those used for the experimental specimen, that is, simply supported constraints. A gradually increasing load was applied at the mid-span, and the mid-span displacement was recorded. The solution process employed a static solver with geometric nonlinearity activated. The resulting load–displacement curves, with the peaks representing the ultimate loads, are shown in Figure 16. A comparison of the ultimate loads for the three cases is provided in Table 3; it is evident that the structural load-carrying capacity aligns more closely with the actual value following the damage update. The error between the ultimate load-carrying capacity of the updated FE model and the actual value is approximately 3.6%. Additionally, the difference in the maximum stress values before and after the model update is 20.5%.

Due to the direct relationship between mesh density and update accuracy, achieving high accuracy in damage updates often requires mesh elements at the millimeter scale or smaller. However, this becomes impractical for FE simulations of large structures, as overly refined meshes significantly increase the number of elements in the model. In addition to the increased element count, this also leads to higher memory and computational resource consumption, potentially making it impossible to run the analysis on standard computers. As shown in Table 4, taking the beam model in this case as an example, the element count in the single-scale model is 95% higher than that in the multiscale model, with a 90% increase in memory usage to achieve the same damage update accuracy. This difference would be even more pronounced in large-scale structures.

5.5. Scale-Up for Whole Structure Analysis. The preceding case study thoroughly illustrates and validates the implementation of the methodology presented in this paper, encompassing both geometrical and structural analysis validation. In this section, the methodology articulated in this paper will be extended and applied to a large-scale full-structure model, demonstrating its adaptability to diverse scenarios. A large prestressed concrete bridge FE model [44], the ChangShan bridge in Dalian, was used as an initial physics-informed FEA model, assuming that the crack

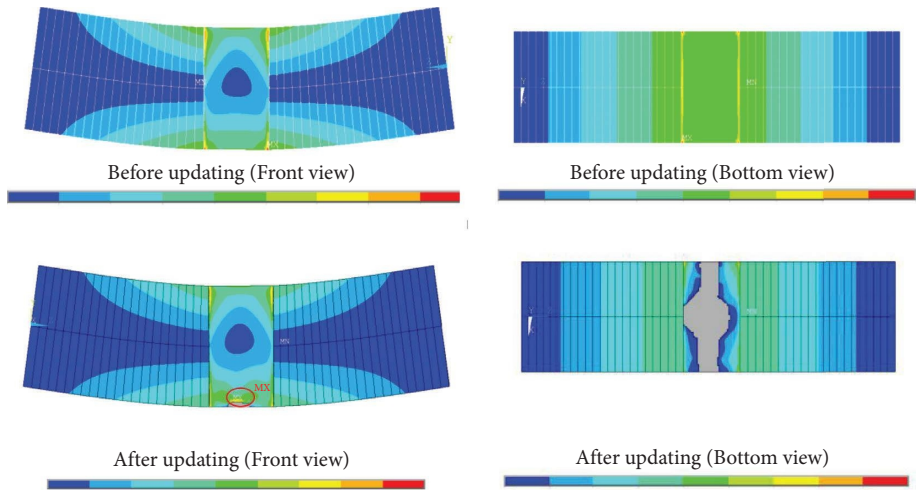

Figure 15: Stress field of incorporating damage into structural analysis.

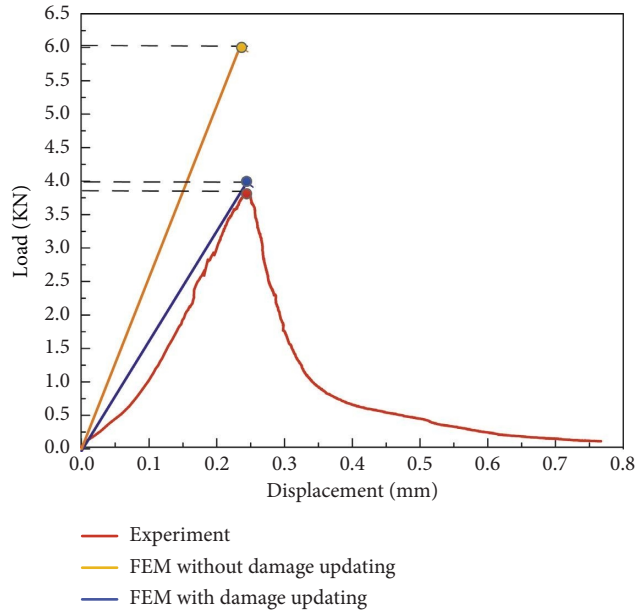

Figure 16: Load–displacement curve.

Table 3: Comparison of mechanical properties before and after FE model update.

Type	Ultimate load (KN)	Maximum stress (MPa)
Experiment results	3.85	—
FEM result (before updating)	6.08	2.88443
FEM result (after updating)	3.99	3.47651

Table 4: Comparison of computational efficiency.

Working condition	Element number	Total memory required as indicated by ANSYS (GB)
Single scale FE model	1,453,500	140
Multi-scale FE model	225,051	14

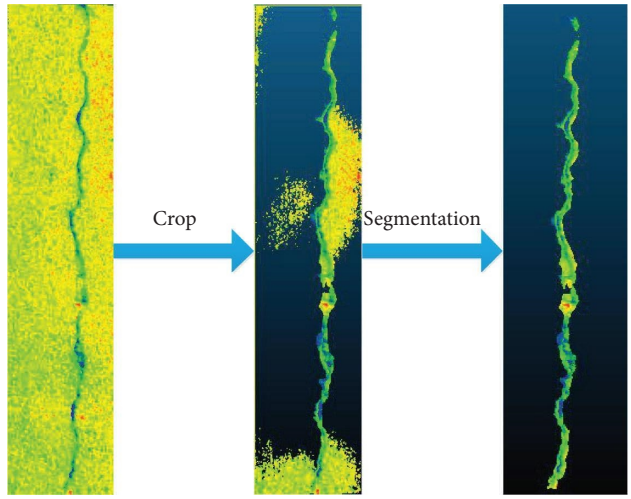

Figure 17: Crack point cloud model extraction.

Figure 18: 3D crack point cloud skeleton.

Table 5: Basic material information for the initial model.

Components	Material	Elastic modulus (MPa)	Poisson ratio	Density (kg/m^3)	Finite element type
Main deck	C55 concrete	3.55×10^4	0.2	2600	BEAM4
Towers	C50 concrete	3.45×10^4	0.2	2600	BEAM188
Cables	Steel cables	1.95×10^5	—	—	LINK10

Table 6: Constraint type for the initial model.

Direction of constraint	X	Y	Z	ROT (X)	ROT (Y)	ROT (Z)
Both ends of the main beam	×	√	√	√	×	×
The base of the bridge tower	√	√	√	√	√	√

Note: √ means constraint, × means no constraint.

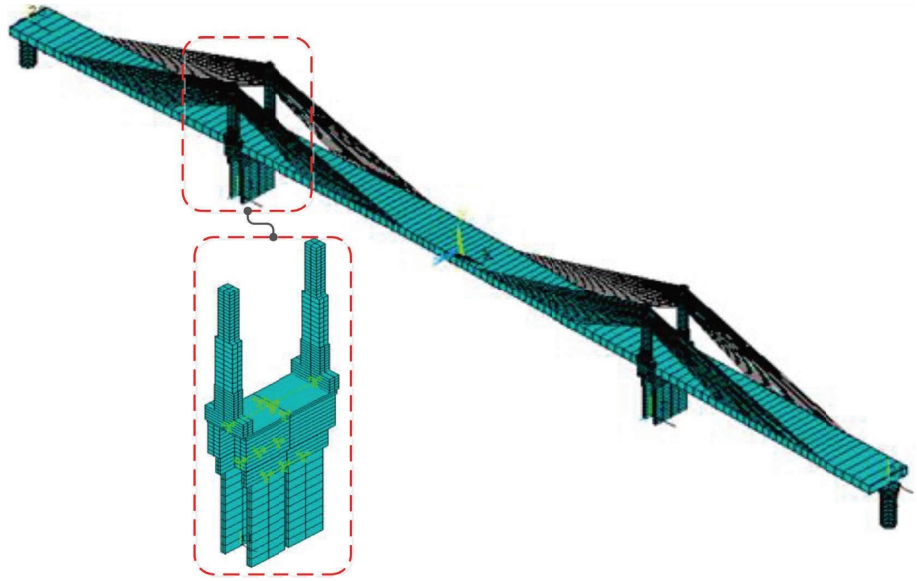

Figure 19: Initial macroscopic finite element model using design parameters.

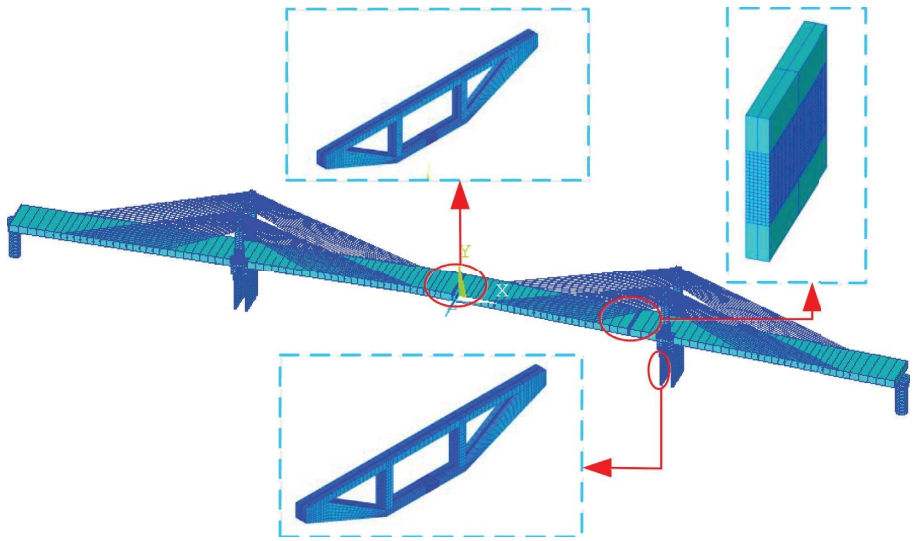

FIGURE 20: The multiscale model with different element types.

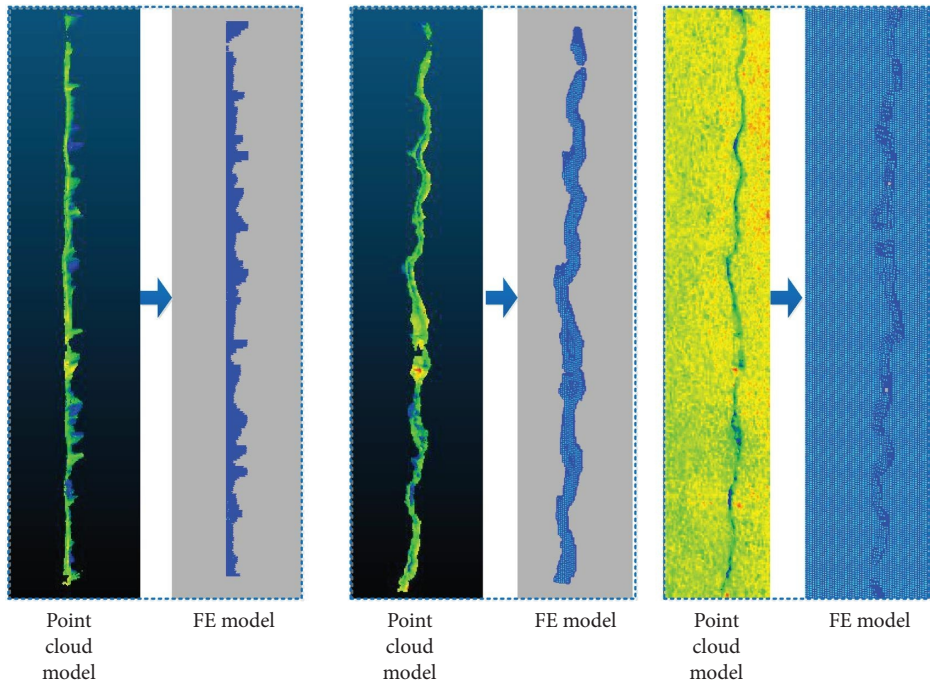

FIGURE 21: Synchronization of cracks from point cloud model to finite element model.

dataset is taken from that bridge [45]. The point cloud processing by the method, as in Section 5.1, is shown in Figure 17. The obtained 3D point cloud skeleton is shown in Figure 18.

The modeling correctness of this FE model has been verified [45], and the modeling process is not described here in detail. The basic information about the bridge is as follows. It is a two-tower, two-cable deck short tower cable-stayed bridge with a main girder arrangement of 540 m (140 + 260+ 140 m). The middle of the bridge adopts a solid structural system of pier, beam, and tower, with a double column concrete tower for the cable-stayed tower and a prestressed concrete streamlined flat box girder for the main girder, with a full girder width of 23 m. In the process of building the initial FE model, the bridge design parameters were used, and their basic information is shown in Tables 5 and 6. The initial FE model is shown in Figure 19. The mesh size of the main beam part is 1–1.5 m in the initial model.

Suppose three cracks are scanned from different locations on the bridge. Synchronization of the DT model is conducted following the same steps as in Case 1. Firstly, a multiscale model of the ChangShan bridge is constructed as depicted in Figure 20. Subsequently, the cracks are integrated into the FE model. Figure 21 illustrates the comparison between the point cloud model of the cracks and the

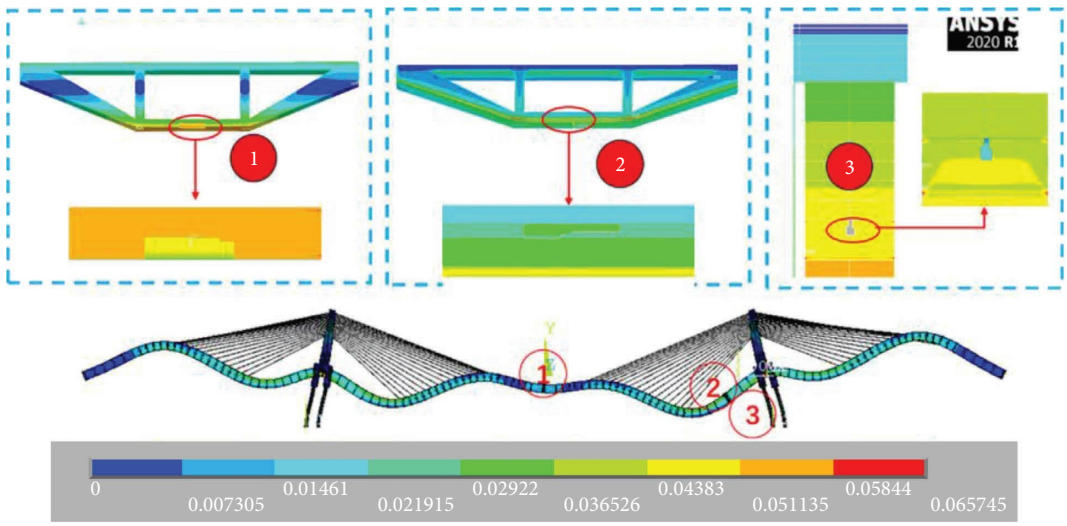

Figure 22: Incorporating crack into structure analysis.

Table 7: Crack size comparison between the point cloud and FE model.

Layer number	Crack depth (cm)	Crack width (cm)			Crack length (cm)		
		Point cloud model	FE model	Error	Point cloud model	FE model	Error
1	$0.27 \le d < 0.28$	4.798	4.8	0.04%	88.585	88.4	0.21%
2	$0.28 \le d < 0.29$	4.955	4.8	3.13%	113.343	96.8	14.60%
3	$0.29 \le d < 0.30$	5.385	5.6	3.99%	113.283	108.8	3.96%
4	$0.30 \le d < 0.31$	6.074	5.6	7.80%	114.23	108.8	4.75%
5	$0.31 \le d < 0.32$	6.78	6.0	11.50%	114.217	108.8	4.74%
6	$0.32 \le d < 0.33$	6.742	6.1	9.52%	114.038	108.4	4.94%
Average error	—		4.65%			5.53%	

FE model. The results of the FE overall displacement and cross-section stress distribution calculations after incorporating the damage into the structural analysis are shown in Figure 22.

To further validate the accuracy of crack synchronization, the point cloud model and the FE model were first compared in terms of damage depth. The damage depth in the point cloud model was 0.3288 cm, while in the FE model, it was 0.3397 cm, resulting in an error of 3.32%. Furthermore, the damage was sliced layer by layer along the depth direction, and comparisons were made regarding its width and length. As shown in Table 7, the average error in crack width was 4.65%, while the average error in crack length was 5.53%.

These errors arise from two main aspects. Firstly, due to nonperfect correspondence between the voxel coordinates of the point cloud and the node coordinates of the FE, a certain margin of error is incorporated into the mapping process. Specifically, the error margins in the length, width, and depth directions during the mapping process are 2 mm, 2 mm, and 1 mm, respectively. Secondly, since the FE model uses 8-node solid elements, based on the computational principle of biased security when a voxel in the point cloud model is mapped to any of the 8 nodes, the element where that node is located will be killed.

6. Discussion and Conclusion

This paper presents a method for synchronizing concrete damage between 3D point cloud data and its PIDT, aiming to create more advanced virtual representations of physical structures to enhance concrete structural assessment. The point cloud data of damage were mapped and incorporated into an FE model using the proposed VNE approach. The FE multiscale and different element regeneration method was used to improve the efficiency of the DT model. The method was validated with two case studies. Based on the study, the following main conclusions may be drawn:

1. A PIDT framework is proposed and implemented not only to provide a more accurate and intuitive visual representation but also to incorporate the mechanical properties of the structure in the cracked or spalled state by directly mapping and updating the damage point cloud information onto a physics-informed model.
2. The VNE method proposed in this paper can effectively improve the accuracy of damage updating and fully reproduce the 3D geometry and direction of damage. The error of the damage volume updated by this method is less than 5% compared with the actual damage volume. At the same time, by this method

damage is incorporated into the structural analysis and localized changes in the mechanical properties of the structure are captured.

3. The proposed method based on multiscale and different element generation provides a solution for updating large and full scale. The method reduces the number of mapping elements, which in turn saves roughly 90% of memory and greatly improves the updating efficiency.
4. The damage updating methodology proposed in this paper is applicable not only at the component level but also at the level of the entire structure.

The research in this paper has to be based on the damage point cloud data obtained utilizing a scanner. In addition, the study focuses on obtaining the mechanical properties of the structure in its current damaged state. In future work, the authors aim to capture the effects of damage on the cyclic behavior of concrete elements—such as crack propagation—while also incorporating reinforcement yielding and fracture into the finite element model update.

Data Availability Statement

The data in this study are available from the corresponding author upon reasonable request.

Conflicts of Interest

The authors declare no conflicts of interest.

Funding

No funding was received for this manuscript. This work was supported by the Fundamental Research Funds for the Central Universities of China, Grant 3132019349, the China Scholarship Council under Grant CSC 202106570014; BIM for Smart Engineering Centre in Cardiff University, UK; Welsh Government Fund (WEFO): "Intelligent Bridge Structure Safety Supported by Physically Informed Digital Twins."

Acknowledgments

This work was supported by the Fundamental Research Funds for the Central Universities of China, Grant 3132019349, the China Scholarship Council under Grant CSC 202106570014; BIM for Smart Engineering Centre in Cardiff University, UK; Welsh Government Fund (WEFO): "Intelligent Bridge Structure Safety Supported by Physically Informed Digital Twins."

References

[1] J. Valença, I. Puente, E. Júlio, H. González-Jorge, and P. Arias-Sánchez, "Assessment of Cracks on Concrete Bridges Using Image Processing Supported by Laser Scanning Survey," *Construction and Building Materials* 146 (2017): 668–678, https://doi.org/10.1016/j.conbuildmat.2017.04.096.

[2] J. Wang, Z. Shi, and M. Nakano, "Strength Degradation Analysis of an Aging RC Girder Bridge Using FE Crack Analysis and Simple Capacity-Evaluation Equations," *Engineering Fracture Mechanics* 108 (2013): 209–221, https://doi.org/10.1016/J.ENGFRACMECH.2013.04.011.

[3] N. M. Telan and A. B. Mehrabi, "Cracked Girders" (2003).

[4] "Overpass Hit and Run Could Cost City of Saskatoon $850K," *CBC News* https://www.cbc.ca/news/canada/saskatoon/overpass-hit-and-run-could-cost-city-850k-1.6527961.

[5] P. Hehenberger and D. Bradley, *Mechatronic Futures: Challenges and Solutions for Mechatronic Systems and Their Designers* (2016).

[6] W. Jia, W. Wang, and Z. Zhang, "From Simple Digital Twin to Complex Digital Twin Part I: A Novel Modeling Method for Multi-Scale and Multi-Scenario Digital Twin," *Advanced Engineering Informatics* 53 (2022): 101706, https://doi.org/10.1016/j.aei.2022.101706.

[7] O. Moztarzadeh, M. Jamshidi, S. Sargolzaei, et al., "Metaverse and Medical Diagnosis: A Blockchain-Based Digital Twinning Approach Based on MobileNetV2 Algorithm for Cervical Vertebral Maturation," *Diagnostics* 13, no. 8 (2023): 1485, https://doi.org/10.3390/diagnostics13081485.

[8] M. Blomfors, C. G. Berrocal, K. Lundgren, and K. Zandi, "Incorporation of Pre-Existing Cracks in Finite Element Analyses of Reinforced Concrete Beams Without Transverse Reinforcement," *Engineering Structures* 229 (2021): 111601, https://doi.org/10.1016/J.ENGSTRUCT.2020.111601.

[9] H. Hu, J. Wang, C. Z. Dong, J. Chen, and T. Wang, "A Hybrid Method for Damage Detection and Condition Assessment of Hinge Joints in Hollow Slab Bridges Using Physical Models and Vision-Based Measurements," *Mechanical Systems and Signal Processing* 183 (2023): 109631, https://doi.org/10.1016/j.ymssp.2022.109631.

[10] M. B. Jamshidi, S. Sargolzaei, S. Foorginezhad, and O. Moztarzadeh, "Metaverse and Microorganism Digital Twins: A Deep Transfer Learning Approach," *Applied Soft Computing* 147 (2023): 110798, https://doi.org/10.1016/j.asoc.2023.110798.

[11] M. B. Jamshidi, S. Lotfi, H. Siahkamari, T. Blecha, J. Talla, and Z. Peroutka, "An Intelligent Digital Twinning Approach for Complex Circuits," *Applied Soft Computing* 154 (2024): 111327, https://doi.org/10.1016/j.asoc.2024.111327.

[12] S. Honghong, Y. Gang, L. Haijiang, Z. Tian, and J. Annan, "Digital Twin Enhanced BIM to Shape Full Life Cycle Digital Transformation for Bridge Engineering," *Automation in Construction* 147 (2023): 104736, https://doi.org/10.1016/j.autcon.2022.104736.

[13] V. Saback, C. Popescu, T. Blanksvärd, and B. Täljsten, "Asset Management of Existing Concrete Bridges Using Digital Twins and BIM: A State-of-the-Art Literature Review," *Nordic Concrete Research* 66, no. 1 (2022): 91–111, https://doi.org/10.2478/ncr-2021-0020.

[14] F. Ghahari, N. Malekghaini, H. Ebrahimian, and E. Taciroglu, "Bridge Digital Twinning Using an Output-Only Bayesian Model Updating Method and Recorded Seismic Measurements," *Sensors* 22, no. 3 (2022): 1278, https://doi.org/10.3390/s22031278.

[15] O. Khalaj, M. Jamshidi, P. Hassas, B. Mašek, C. Štadler, and J. Svoboda, "Digital Twinning of a Magnetic Forging Holder to Enhance Productivity for Industry 4.0 and Metaverse," *Processes* 11, no. 6 (2023): 1703, https://doi.org/10.3390/pr11061703.

[16] V. Hoskere, Y. Narazaki, and B. F. Spencer, "Digital Twins as Testbeds for Vision-Based Post-Earthquake Inspections of

Buildings," in *Lecture Notes in Civil Engineering* (Springer Science and Business Media Deutschland GmbH, 2023), 485–495, https://doi.org/10.1007/978-3-031-07258-1_50.

[17] Y. A. Yucesan and F. A. C. Viana, "Physics-Informed Digital Twin for Wind Turbine Main Bearing Fatigue: Quantifying Uncertainty in Grease Degradation," *Applied Soft Computing* 149 (2023): 110921, https://doi.org/10.1016/j.asoc.2023.110921.

[18] K. Yun, Z. Wang, L. He, and J. Liu, "A Damage Model Based on the Introduction of a Crack Direction Parameter for FRP Composites Under quasi-static Load," *Composite Structures* 184 (2018): 388–399, https://doi.org/10.1016/J.COMPSTRUCT.2017.09.099.

[19] F. Tao, F. Sui, A. Liu, et al., "Digital Twin-Driven Product Design Framework," *International Journal of Production Research* 57, no. 12 (2018): 3935–3953, https://doi.org/10.1080/00207543.2018.1443229.

[20] Z. Mousavi, S. Varahram, M. M. Ettefagh, M. H. Sadeghi, W. Q. Feng, and M. Bayat, "A Digital Twin-Based Framework for Damage Detection of a Floating Wind Turbine Structure Under Various Loading Conditions Based on Deep Learning Approach," *Ocean Engineering* 292 (2024): 116563, https://doi.org/10.1016/j.oceaneng.2023.116563.

[21] S. H. Radbakhsh, M. Nik-Bakht, and K. Zandi, "Structural Digital Twin of Concrete Infrastructure Powered With Physics-Informed Neural Networks," in *RILEM Bookseries* (Springer Science and Business Media B.V, 2024), 1101–1113, https://doi.org/10.1007/978-3-031-53389-1_97.

[22] Y. j. Huang, S. Natarajan, H. Zhang, et al., "A CT Image-Driven Computational Framework for Investigating Complex 3D Fracture in Mesoscale Concrete," *Cement and Concrete Composites* 143 (2023): 105270, https://doi.org/10.1016/j.cemconcomp.2023.105270.

[23] Y. j. Huang, Z. s. Zheng, F. Yao, et al., "Arbitrary Polygon-Based CSFEM-PFCZM for Quasi-Brittle Fracture of Concrete," *Computer Methods in Applied Mechanics and Engineering* 424 (2024): 116899, https://doi.org/10.1016/j.cma.2024.116899.

[24] Y. Huang, Z. Yang, W. Ren, G. Liu, and C. Zhang, "3D Meso-Scale Fracture Modelling and Validation of Concrete Based on In-Situ X-Ray Computed Tomography Images Using Damage Plasticity Model," *International Journal of Solids and Structures* 67–68 (2015): 340–352, https://doi.org/10.1016/j.ijsolstr.2015.05.002.

[25] S. Jiang, Y. Cheng, and J. Zhang, "Vision-Guided Unmanned Aerial System for Rapid Multiple-Type Damage Detection and Localization," *Structural Health Monitoring* 22, no. 1 (2023): 319–337, https://doi.org/10.1177/14759217221084878.

[26] S. Wang, C. Rodgers, G. Zhai, et al., "A Graphics-Based Digital Twin Framework for Computer Vision-Based Post-Earthquake Structural Inspection and Evaluation Using Unmanned Aerial Vehicles," *Journal of Infrastructure Intelligence and Resilience* 1 (2022): 100003, https://doi.org/10.1016/j.iintel.2022.100003.

[27] X. Zhou, K. Sun, J. Wang, et al., "Computer Vision Enabled Building Digital Twin Using Building Information Model," *IEEE Transactions on Industrial Informatics* 19, no. 3 (2023): 2684–2692, https://doi.org/10.1109/TII.2022.3190366.

[28] R. Lu and I. Brilakis, "Digital Twinning of Existing Reinforced Concrete Bridges From Labelled Point Clusters," *Automation in Construction* 105 (2019): 102837, https://doi.org/10.1016/j.autcon.2019.102837.

[29] C. Zhang, J. Shu, Y. Shao, and W. Zhao, "Automated Generation of FE Models of Cracked RC Beams Based on 3D Point Clouds and 2D Images," *Journal of Civil Structural Health Monitoring* 12, no. 1 (2022): 29–46, https://doi.org/10.1007/s13349-021-00525-5.

[30] D. Loverdos and V. Sarhosis, "Image2DEM: A Geometrical Digital Twin Generator for the Detailed Structural Analysis of Existing Masonry Infrastructure Stock," *SoftwareX* 22 (2023): 101323, https://doi.org/10.1016/j.softx.2023.101323.

[31] F. Jiang, L. Ma, T. Broyd, and K. Chen, "Digital Twin and Its Implementations in the Civil Engineering Sector," *Automation in Construction* 130 (2021): 103838, https://doi.org/10.1016/j.autcon.2021.103838.

[32] V. Stojanovic, M. Trapp, R. Richter, B. Hagedorn, and J. Döllner, "Towards the Generation of Digital Twins for Facility Management Based on 3D Point Clouds" (2018).

[33] H. H. Hosamo and M. H. Hosamo, "Digital Twin Technology for Bridge Maintenance Using 3D Laser Scanning: A Review," *Advances in Civil Engineering* 2022, no. 1 (2022): https://doi.org/10.1155/2022/2194949.

[34] L. Barazzetti, "Parametric As-Built Model Generation of Complex Shapes From Point Clouds," *Advanced Engineering Informatics* 30, no. 3 (2016): 298–311, https://doi.org/10.1016/j.aei.2016.03.005.

[35] S. Chen, G. Fan, and J. Li, "Improving Completeness and Accuracy of 3D Point Clouds by Using Deep Learning for Applications of Digital Twins to Civil Structures," *Advanced Engineering Informatics* 58 (2023): 102196, https://doi.org/10.1016/j.aei.2023.102196.

[36] L. Cui, L. Zhou, Q. Xie, et al., "Direct Generation of Finite Element Mesh Using 3D Laser Point Cloud," *Structures* 47 (2023): 1579–1594, https://doi.org/10.1016/j.istruc.2022.12.010.

[37] K. Yu, C. Zhang, M. Shooshtarian, W. Zhao, and J. Shu, "Automated Finite Element Modeling and Analysis of Cracked Reinforced Concrete Beams From Three Dimensional Point Cloud," *Structural Concrete* 22, no. 6 (2021): 3213–3227, https://doi.org/10.1002/suco.202100194.

[38] Q. Kong, J. Gu, B. Xiong, and C. Yuan, "Vision-Aided Three-Dimensional Damage Quantification and Finite Element Model Geometric Updating for Reinforced Concrete Structures," *Computer-Aided Civil and Infrastructure Engineering* 38, no. 17 (2023): 2378–2390, https://doi.org/10.1111/mice.12967.

[39] M. S. Alam and M. A. Wahab, "Modeling the Fatigue Crack Growth and Propagation Life of a Joint of Two Elastic Materials Using Interface Elements," *International Journal of Pressure Vessels and Piping* 82, no. 2 (2005): 105–113, https://doi.org/10.1016/J.IJPVP.2004.07.017.

[40] S. M. Hoseyni, "Verifying the Effect of Element Birth and Death Technique on Stress Distribution in Cracked Areas," https://www.researchgate.net/publication/314305064.

[41] R. J. Guyan, "Reduction of Stiffness and Mass Matrices," *AIAA Journal* 3, no. 2 (1965): 380, https://doi.org/10.2514/3.2874.

[42] "CloudCompare," https://www.danielgm.net/cc/.

[43] "ANSYS," https://www.ansys.com/.

[44] G. Y. Y. J. Honghong Song, "Analyses of Able-Stayed Bridges' Static Wind Stability and Pulsating Wind Buffeting Based on ANSYS," *Earthquake Engineering and Engineering Dynamics* 39 (2019): 83–90, https://doi.org/10.13197/j.eeev.2019.06.83songhh.012.

[45] P. Stałowska, C. Suchocki, and M. Rutkowska, "Crack Detection in Building Walls Based on Geometric and Radiometric Point Cloud Information," *Automation in Construction* 134 (2022): 104065, https://doi.org/10.1016/J.AUTCON.2021.104065.